A spectral/finite difference method for simulating large deformations of heterogeneous, viscoelastic materials

S. M. Schmalholz,* Y. Y. Podladchikov and D. W. Schmid

Geologisches Institut, ETH Zentrum, 8092 Zürich, Switzerland. E-mail: stefan@erdw.ethz.ch

SUMMARY

A numerical algorithm is presented that simulates large deformations of heterogeneous, viscoelastic materials in two dimensions. The algorithm is based on a spectral/finite difference method and uses the Eulerian formulation including objective derivatives of the stress tensor in the rheological equations. The viscoelastic rheology is described by the linear Maxwell model, which consists of an elastic and viscous element connected in series. The algorithm is especially suitable to simulate periodic instabilities. The derivatives in the direction of periodicity are approximated by spectral expansions, whereas the derivatives in the direction orthogonal to the periodicity are approximated by finite differences. The 1-D Eulerian finite difference grid consists of centre and nodal points and has variable grid spacing. Time derivatives are approximated with finite differences using an implicit strategy with a variable time step. The performance of the numerical code is demonstrated by calculation, for the first time, of the pressure field evolution during folding of viscoelastic multilayers. The algorithm is stable for viscosity contrasts up to 5×10^5, which demonstrates that spectral methods can be used to simulate dynamical systems involving large material heterogeneities. The successful simulations show that combined spectral/finite difference methods using the Eulerian formulation are a promising tool to simulate mechanical processes that involve large deformations, viscoelastic rheologies and strong material heterogeneities.

Key words: deformation, finite difference methods, inhomogeneous media, numerical techniques, spectral methods, viscoelasticity.

INTRODUCTION

In geological environments many dynamic processes such as folding and thermal convection are characterized by large deformations (e.g. Johnson & Fletcher 1994; Turcotte & Schubert 1982). Also, deformed geological materials are often heterogeneous and show viscoelastic behaviour (e.g. Fowler 1990; Ramsay & Huber 1987; Turcotte & Schubert 1982). Therefore, the simulation of dynamic geological processes using numerical methods requires suitable algorithms that can handle simultaneously large deformations, strong material heterogeneities and viscoelastic rheologies. Numerical simulations are necessary to understand the physics and mechanics of geological processes. They are an important additional tool to analytical solutions and analogue experiments, because analytical solutions are generally limited to small deformations and simple geometries and rheologies, whereas analogue experiments are unsuitable to monitor the pressure field evolution or to scale elastic properties. However, suitable numerical algorithms, especially for the simul-

taneous treatment of heterogeneities, complex rheologies and large deformations, are still rare and the development of suitable algorithms is of great interest.

In this study a numerical algorithm is presented that can simulate large deformations of heterogeneous, viscoelastic materials. The algorithm is based on the Eulerian formulation (e.g. Sedov 1994). It involves objective derivatives of the stress tensor and a combination of viscous flow and elasticity as a Maxwell body rheology for stress deviators (e.g. Harder 1991; Huilgol & Phan-Thien 1997; Simo & Hughes 1998). The algorithm is developed with the specific goal of treating periodic instabilities such as folding, thermal convection and Rayleigh–Taylor instabilities (e.g. Turcotte & Schubert 1982). The natural technique to exploit this periodicity is to employ spectral decomposition for numerical discretization. In the spectral method, the solution of a differential equation is approximated by a truncated series of trigonometric functions (e.g. Canuto *et al.* 1988; Fornberg 1996). The global nature of the spectral method permits high accuracy with only a few terms in the approximate solution (e.g. Fletcher 1997a). Spectral methods are frequently used in fluid dynamics (e.g. Canuto *et al.* 1988) and have been applied successfully to simulate

* Now at: Geomodelling Solutions Gmbtl, Binzstvasse 18, 8045 Zürich, Switzerland.

mantle convection (e.g. Balachandar & Yuen 1994; Tackley *et al.* 1993). For the algorithm presented in this study, discretization by spectral methods is performed only in the direction of the periodic instability, and finite difference (FD) methods (e.g. Fletcher 1997a; Shashkov 1996) are used orthogonal to this direction. FD methods have been applied for example to study thermal convection of viscoelastic materials (e.g. Harder 1991).

The aims of this paper are (i) to document the developed numerical algorithm based on the spectral/finite difference method and (ii) to demonstrate the performance of the algorithm by simulating folding of viscoelastic multilayers. Folding is a common response of layered rocks to deformation and the resulting geological structures, termed folds, frequently occur in nature on all spatial scales (e.g. Biot 1965; Johnson & Fletcher 1994; Ramberg 1981). Numerical simulations of folding have been performed using finite element methods (e.g. Cobbold 1977; Dieterich 1970; Lan & Hudleston 1995; Mancktelow 1999) and FD methods (e.g. Zhang *et al.* 1996). However, most numerical simulations only modelled the geometrical evolution of single-layer folds and simulations of the stress and pressure field evolution within viscoelastic multilayers do, to the best of our knowledge, not exist (for the pressure field evolution in viscoelastic single layers see Schmalholz & Podladchikov 1999).

FORMULATION OF GOVERNING EQUATIONS

The deformation of the heterogeneous, viscoelastic material is simulated in two dimensions for plane strain, incompressible materials and in the absence of gravity. The four unknown functions are v_x, v_y, τ_{xx} and τ_{xy}, where v_x and v_y are the velocities in the x- and y-directions, respectively, and τ_{xx} and τ_{xy} are the x-component of the deviatoric stress tensor and the shear stress component, respectively. All four unknown functions are dependent on x, y and t, where x, y and t are the coordinate in the x-direction, the coordinate in the y-direction and the time, respectively (Fig. 1). Four governing equations are required to form a closed system of equations. The first governing equation is built from the equilibrium equations

Figure 1. Boundary conditions for viscoelastic folding. Constant velocities are applied on free-slipping boundaries.

(e.g. Mase 1970; Sedov 1994), which are given by

$$-\frac{\partial p}{\partial x} + \frac{\partial \tau_{xx}}{\partial x} + \frac{\partial \tau_{xy}}{\partial y} = 0\,, \tag{1}$$

$$-\frac{\partial p}{\partial y} - \frac{\partial \tau_{xx}}{\partial y} + \frac{\partial \tau_{xy}}{\partial x} = 0\,, \tag{2}$$

where p is the pressure and the relation $\tau_{xx} = -\tau_{yy}$ (due to incompressibility) is used. The two equilibrium equations are combined into one equation by taking the partial derivative of eq. (1) with respect to y and the partial derivative of eq. (2) with respect to x and subtracting eq. (2) from eq. (1). This process also eliminates the pressure and the total number of unknowns remains four. The combined equilibrium equation is then

$$2\frac{\partial^2}{\partial y \partial x}\tau_{xx} + \left(\frac{\partial^2}{\partial y^2} - \frac{\partial^2}{\partial x^2}\right)\tau_{xy} = 0\,. \tag{3}$$

The next two governing equations are obtained by the rheological stress–strain rate relationships for a linear viscoelastic material described by the Maxwell body (e.g. Huilgol & Phan-Thien 1997; Simo & Hughes 1998). These equations for the deviatoric stresses are given by

$$\dot{\varepsilon}_{xx} = \frac{\tau_{xx}}{2\mu} + \frac{1}{2G}\frac{D\tau_{xx}}{Dt}\,, \tag{4}$$

$$\dot{\varepsilon}_{xy} = \frac{\tau_{xy}}{2\mu} + \frac{1}{2G}\frac{D\tau_{xy}}{Dt}\,, \tag{5}$$

where

$$\dot{\varepsilon}_{xx} = \frac{\partial v_x}{\partial x}\,; \qquad \dot{\varepsilon}_{xy} = \frac{1}{2}\left(\frac{\partial v_x}{\partial y} + \frac{\partial v_y}{\partial x}\right) \tag{6}$$

and μ and G are the viscosity and the shear modulus of the material, respectively.

One step in formulating the rheological equation for a viscoelastic material, discussed in more detail in the following, is the application of the differential operator D/Dt, which is the absolute time derivative of a tensor of rank 2 given in material or Lagrangian coordinates (e.g. Aris 1962; Oldroyd 1950; Sedov 1994). As a principle of rheology, the constitutive equations (4) and (5) must be independent of the reference system (principle of objectivity or frame indifference) (e.g. Simo & Hughes 1998). Therefore, tensors used in the formulation of the constitutive equations have tensor components that are defined for material or Lagrangian coordinates, that is, for coordinates fixed to the material. This makes the constitutive equations independent of all observer coordinate systems. The stress state of a 2-D material is described by a stress tensor field that consists of individual stress tensors defined for particular points of the material. The components of each stress tensor depend on the base vectors that define the local coordinate system at each particular point. Two factors complicate the formulation of the viscoelastic rheological equation that can be used for discretization.

First, on curved surfaces, such as the boundary of a folded layer, there are several possibilities to establish a local Cartesian coordinate system, namely by using contravariant or covariant base vectors (e.g. Borisenko & Tarapov 1968; Eisenhart 1997; Kreyszig 1991). The stress tensor components are different if the local coordinate system is defined by either contravariant or covariant base vectors, or by a combination of contravariant and covariant base vectors (mixed formulation). However, it
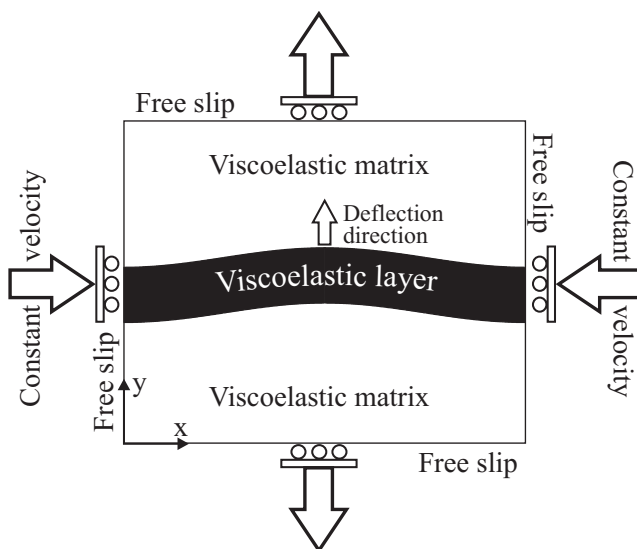
is still an open question whether the stress tensor has to be a contravariant, covariant or mixed tensor (e.g. Huilgol & Phan-Thien 1997; Sedov 1960). In this study, the stress tensor is taken to be contravariant.

Second, the spatial derivatives of the stress tensor appear in the constitutive equation due to the absolute time derivative of the stress tensor. The time derivative of any time-dependent tensor of rank 2 [here $\mathbf{T}(t,\mathbf{x}(t))$] given in Eulerian coordinates [here $\mathbf{x}(t)$] is given by using the chain rule of differentiation,

$$\frac{D\mathbf{T}(t,\mathbf{x}(t))}{Dt} = \frac{\partial \mathbf{T}(t,\mathbf{x}(t))}{\partial t} + \frac{\partial \mathbf{T}(t,\mathbf{x}(t))}{\partial \mathbf{x}(t)} \cdot \frac{\partial \mathbf{x}(t)}{\partial t}. \tag{7}$$

This derivative is also called the material, substantial or comoving derivative (e.g. Mase 1970). Eq. (7) only holds for Euclidean spaces (e.g. Borisenko & Tarapov 1968; Eisenhart 1997) and has to be expanded for non-Euclidean or curved spaces as, for example, defined by the fold boundaries. The reason for this is that the local base vectors vary along curved surfaces and this change of the base vectors in space must be taken into account while calculating the spatial derivative of the stress tensor components. The spatial derivative of tensors of rank 2 is called the covariant derivative in non-Euclidean spaces (e.g. Aris 1962; Sedov 1994). Tensors of rank 2 have different covariant derivatives if their tensor components are defined for contravariant, covariant or mixed base vectors.

The application of D/Dt is also known as convective or convected differentiation (Oldroyd 1950). The convected derivative of a contravariant tensor of rank 2 given for Eulerian coordinates is called the contravariant or upper convected derivative, and after application of convected differentiation, eqs (4) and (5) can be written as (e.g. Huilgol & Phan-Thien 1997)

$$\dot{\varepsilon}_{xx} = \frac{\tau_{xx}}{2\mu} + \frac{1}{2G}\left(\frac{\partial \tau_{xx}}{\partial t} + v_x \frac{\partial \tau_{xx}}{\partial x} + v_y \frac{\partial \tau_{xx}}{\partial y} - 2\tau_{xy} \frac{\partial v_x}{\partial y} - 2\tau_{xx} \frac{\partial v_x}{\partial x} \right), \tag{8}$$

$$\dot{\varepsilon}_{xy} = \frac{\tau_{xy}}{2\mu} + \frac{1}{2G}\left(\frac{\partial \tau_{xy}}{\partial t} + v_x \frac{\partial \tau_{xy}}{\partial x} + v_y \frac{\partial \tau_{xy}}{\partial y} + \tau_{xx} \frac{\partial v_x}{\partial y} - \tau_{xx} \frac{\partial v_y}{\partial x} \right). \tag{9}$$

All terms, involving both velocities and stresses, in eqs (8) and (9) are quasi-non-linear, because the deviatoric stresses are functions of the velocities. The rheological equations (8) and (9), describing a linear viscoelastic Maxwell fluid, are now given for Eulerian coordinates but are still objective, that is, independent of the reference system.

The fourth governing equation used is the continuity equation describing the incompressibility of the material and is written as

$$\frac{\partial v_x}{\partial x} + \frac{\partial v_y}{\partial y} = 0. \tag{10}$$

Thus the four equations (3), (8), (9) and (10) form a closed system of partial differential equations for the four unknown functions v_x, v_y, τ_{xx} and τ_{xy}.

BOUNDARY CONDITIONS FOR FOLDING

Folding is the lateral (that is, orthogonal to the compression direction) deflection of an embedded layer due to layer-parallel compression (e.g. Biot 1965; Ramberg 1981). Folding of a

viscoelastic layer embedded in a finite viscoelastic matrix is sketched in Fig. 1. At the boundaries the velocities in the x- and y-directions are constant (pure shear deformation). The shear stresses at the boundaries of the area considered are zero (free slip). The boundaries between layer and matrix are connected, which prevents free slip between layer and matrix and therefore layer-parallel shear is included.

NUMERICAL IMPLEMENTATION

Time derivatives are approximated with FDs implicit in time using a variable time step dt, e.g.

$$\frac{\partial \tau_{xx}}{\partial t} = \frac{\tau_{xx} - \tau_{xx}^{\text{old}}}{dt}, \tag{11}$$

where τ_{xx} and τ_{xx}^{old} are the new and old stress components, respectively. Substituting eq. (11) into eqs (8) and (9) and solving both equations for new stress components yields e.g. (*cf.* eq. 8)

$$\tau_{xx} = 2\mu_{\text{eff}} \frac{\partial v_x}{\partial x} + \eta_{\text{eff}}\left[\tau_{xx}^{\text{old}} - dt\left(v_x \frac{\partial \tau_{xx}^{\text{old}}}{\partial x} + v_y \frac{\partial \tau_{xx}^{\text{old}}}{\partial y} \right. \right.$$
$$\left. \left. -2\tau_{xy}^{\text{old}} \frac{\partial v_x}{\partial y} - 2\tau_{xx}^{\text{old}} \frac{\partial v_x}{\partial x} \right) \right], \tag{12}$$

where

$$\mu_{\text{eff}} = \frac{1}{\dfrac{1}{\mu} + \dfrac{1}{Gdt}} \qquad \text{and} \qquad \eta_{\text{eff}} = \frac{1}{1 + \dfrac{Gdt}{\mu}}. \tag{13}$$

The coefficients μ_{eff} and η_{eff} are time-step-dependent effective viscosities.

The periodic behaviour of folding in the shortening (x-) direction and the pure shear boundary conditions allow us to approximate the x-dependence of the velocities, stress components and effective viscosities with simple (i.e. only cosine or sine) spectral expansions, e.g.

$$v_y = \sum_{k=0}^{nk}\left\{ vy_k(y)\cos(kwx)\left(1 - \frac{k}{nk+1}\right) \right\}, \tag{14}$$

$$v_x = -\sum_{k=0}^{nk}\left\{ \frac{\frac{\partial}{\partial y} vy_k(y)\sin(kwx)}{kw}\left(1 - \frac{k}{nk+1}\right) \right\}, \tag{15}$$

$$\tau_{xx} = \sum_{k=0}^{nk}\left\{ \tau xx_k(y)\cos(kwx)\left(1 - \frac{k}{nk+1}\right) \right\}, \tag{16}$$

$$\mu_{\text{eff}} = \sum_{i=0}^{2nk}\left\{ \mu_i(y)\cos(iwx)\left(1 - \frac{i}{2nk+1}\right) \right\}. \tag{17}$$

Here nk is the number of summands or 'harmonics' within the approximation series and w is the frequency. The velocity in the x-direction is expressed through the velocity in the y-direction (eq. 15) using the continuity equation (10). The harmonic coefficients [e.g. $vy_k(y)$] are only dependent on y and the cosines and sines are only dependent on x. This allows a separate treatment of derivatives with respect to x and y. The derivatives with respect to x are now trivial, because the x-dependence is described exclusive by trigonometric functions. The factor

$[1-k/(nk+1)]$ is a smoothing factor that may be used (i) to filter out oscillations due to the Gibbs phenomenon (e.g. Fornberg 1996) and (ii) to accelerate convergence of the trigonometric series (eqs 14–17).

The expressions for the stress components (e.g. eq. 12) include multiplications of trigonometric series (convolution) after substituting the spectral expansions for the velocities, stress components and effective viscosities. For the multiplication of any two spectral expressions we use exact trigonometric relationships such as
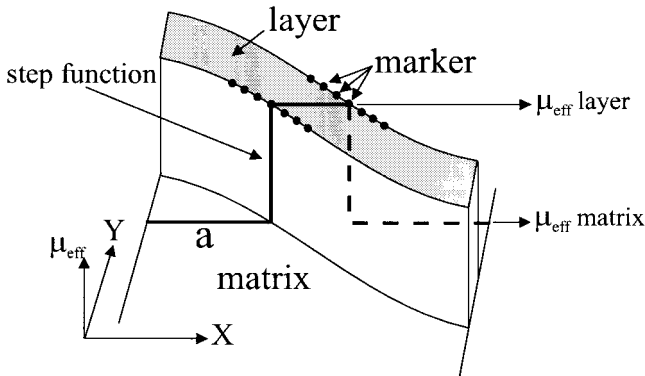
$$\sum_i vy_i \cos(iwx) \sum_m \mu_m \cos(mwx)$$

$$= \frac{1}{2} \sum_i \sum_m \{vy_i \mu_m \cos(mwx + iwx)$$

$$+ vy_i \mu_m \cos(-mwx + iwx)\}, \qquad (18)$$

where vy_i and μ_m are velocity and effective viscosity harmonics, respectively. The velocity harmonics vy_i are unknown, whereas the viscosity harmonics μ_m are known. To set up a system of equations, the coefficients vy_i and μ_m have to be collected in front of one specific cosine, say $\cos(kwx)$. Furthermore, the known coefficients μ_m have to be collected in front of the unknown velocity harmonics vy_i. There are four possibilities to produce a cosine with harmonic number k on the right-hand side of eq. (18), namely by substituting the index m of the known coefficients μ_m with $m=-i+k$, $m=-i-k$, $m=i+k$ and $m=i-k$. These four coefficients are collected in front of vy_i and summing now over k instead of m transforms the right-hand side of eq. (18) into

$$\frac{1}{2} \sum_i \sum_k [-\mu_{-i-k} - \mu_{-i+k} - \mu_{i-k} - \mu_{i+k}]vy_i \cos(kwx). \qquad (19)$$

The effective viscosity harmonics are now collected as coefficients in front of the velocity harmonics, which must be determined. Effective viscosity harmonics with a negative index are dropped.

The harmonics of the effective viscosities are known and calculated directly from the positions of the layer boundaries using analytical expressions (Fig. 2). The profile of the effective

viscosities in the x-direction across the layer can be described using step functions (Fig. 2). These step functions, f, can be approximated by a series expansion with

$$f = \mu_0 + \sum_{k=1}^{nk} \mu_k, \qquad (20)$$

where for example for a step from low to high effective viscosity at the position $x=a$,

$$\mu_0 = \mu_{\text{matrix}} + \frac{2a}{\lambda} (\mu_{\text{layer}} - \mu_{\text{matrix}}) \qquad (21)$$

and

$$\frac{4}{\lambda kw} (\mu_{\text{layer}} - \mu_{\text{matrix}}) \left[\sin(akw) \cos(kwx) \left(1 - \frac{k}{nk+1} \right) \right]. \qquad (22)$$

Here λ is the wavelength and a is the distance from the origin of the x-coordinate to the x-coordinate of the corresponding marker on the layer boundary (Fig. 2). The layer boundary is described by marker points, which are fixed to this boundary.

The general structure of the stress harmonics τxx_k and τxy_k can be expressed as a sum of velocity harmonics, derivatives of velocity harmonics with respect to y and old stress harmonics, and all summands are multiplied by 'rheological' coefficients (*cf.* eq. 12), e.g.
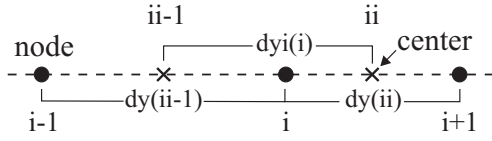
$$\tau xx_k(y)$$

$$= \sum_{m=0}^{nk} \left\{ \begin{array}{l} RCxx1_{k,m}(y)vy_m(y) + RCxx2_{k,m}(y) \dfrac{\partial vy_m(y)}{\partial y} \\[2mm] + RCxx3_{k,m}(y) \dfrac{\partial^2 vy_m(y)}{\partial y^2} + RCxx4_{k,m}(y)\tau xx_m^{\text{old}}(y) \end{array} \right\}, \qquad (23)$$

where $RCxx1_{k,m}$ to $RCxx4_{k,m}$ are rheological coefficients dependent on y given by

$$RCxx1_{k,m}(y) = 0,$$

$$RCxx2_{k,m}(y) = -\mu_{-m-k}(y) - \mu_{-m+k}(y) - \mu_{m-k}(y) - \mu_{m+k}(y),$$

$$RCxx3_{k,m}(y) = 0,$$

$$RCxx4_{k,m}(y) = \frac{1}{2} (\eta_{-m-k}(y) + \eta_{-m+k}(y) + \eta_{m-k}(y) + \eta_{m+k}(y)). \qquad (24)$$

The rheological coefficients presented above are valid for a rheological equation without advective and objective terms, because the coefficients for the full upper convected Maxwell equation would cover several pages.

The non-periodic behaviour in the amplification (y-) direction is approximated with a conservative FD method using a variable, staggered grid (e.g. Fletcher 1997b; Shashkov 1996). A grid is called staggered if it consists of nodes and centres (Fig. 3). The harmonics of τ_{xx} are defined at the centre points of the y-grid and all other variables are defined at the nodal points to obtain the same approximation structure for all FD expressions. The discretized equilibrium equation (3) is

Figure 2. Effective viscosity profile across a folded layer. The profile describes a step function with two steps if the layer with a higher effective viscosity (μ_{eff}) than the matrix is crossed. The step function is used to calculate the effective viscosity harmonics, which are the Fourier coefficients of the step function. With this approach, any heterogeneous pattern can be simulated with a spectral method.

Figure 3. The variable, staggered grid in the *y*-direction. Nodes are numbered with index *i* and centres with index *ii*. The distance between two nodes is termed *dy* and has the index of the centre between these two nodes. The distance between two centres is termed *dyi* and has the index of the node between these two centres.

given as

$$-2\frac{(\tau xx_k(ii) - \tau xx_k(ii-1))kw}{dyi(i)}$$

$$+\frac{\dfrac{\tau xy_k(i+1) - \tau xy_k(i)}{dy(ii)} - \dfrac{\tau xy_k(i) - \tau xy_k(i-1)}{dy(ii-1)}}{dyi(i)}$$

$$+ \tau xy_k(i)k^2w^2 = 0, \qquad (25)$$

where *i* and *ii* are indices of nodes and centre points, respectively, and $dy(ii)$ and $dyi(i)$ are distances between nodes and centre points, respectively (Fig. 3). The FD expressions for the stress harmonics are given as e.g.

$$\tau xx_k(ii)$$

$$= \sum_{m=0}^{nk} \left\{ \begin{array}{l} RCxx1_{k,m}(ii)vy_m(ii) + RCxx2_{k,m}(ii)\dfrac{\Delta vy_m(ii)}{\Delta y} \\[2mm] + RCxx3_{k,m}(ii)\dfrac{\Delta^2 vy_m(ii)}{\Delta y^2} + RCxx4_{k,m}(ii)\tau xx_m^{\text{old}}(ii) \end{array} \right\},$$

$$(26)$$

where the FD expressions of the first and second velocity derivatives are given as

$$\frac{\Delta vy_k(i)}{\Delta y} = \frac{vy_k(ii) - vy_k(ii-1)}{dyi(i)} \qquad (27)$$

and

$$\frac{\Delta^2 vy_k(i)}{\Delta y^2} = \frac{\dfrac{vy_k(i+1) - vy_k(i)}{dy(ii)} - \dfrac{vy_k(i) - vy_k(i-1)}{dy(ii-1)}}{dyi(i)}, \qquad (28)$$

respectively. The calculation of the stress harmonics requires interpolation of the nodal velocity harmonics either from centre to nodal points or vice versa. Interpolation from nodal to centre points is trivial, but for the interpolation from centre to nodal points the different sizes of the distances between nodal and centre points have to be taken into account for a variable grid. The interpolation rule is given as

$$\tau xx_k(i) = \tau xx_k(ii-1)\frac{1}{2}\frac{dy(ii-1)}{dyi(i)}$$

$$+ \tau xx_k(ii)\left(1 - \frac{1}{2}\frac{dy(ii-1)}{dyi(i)}\right). \qquad (29)$$

After substitution of eqs (29), (28), (27) and (26) and the corresponding expressions for τxy_k into the equilibrium equation (25), the only remaining unknowns are the velocity harmonics $vy_k(i)$ that are multiplied, after performing all derivatives with respect

to *x*, exclusively by sin(*kwx*). The highest derivative with respect to *y* that appears in the equilibrium equation is of order four. The trigonometric functions sin(*kwx*) are linear independent functions and the only way to set the equilibrium equation to zero is to set the coefficients in front of the sin(*kwx*) to zero. This yields a system of $nk \times ny$ linear equations, where *ny* is the number of nodal points used for the FD discretization.

The system is solved iteratively where in the course of the iterations the five main diagonals containing vy_k are kept on the left-hand side within the main diagonal and the other diagonals containing the remaining $vy_{m \neq k}$ contribute to the right-hand-side vector during iterations. This iteration method has a high performance because of (i) the existence of good initial guesses for the iteration procedure, which are the previous time step velocity harmonics, and (ii) the appropriate choice of the functional basis (spectral) for the discretization of periodic instability problems, which results in strong diagonal dominance of the linear system of equations. The resulting system of linear equations, to calculate a certain $vy_k(i)$, has the following general form:

$$Al_{k,k}vy_k(i-2) - Bl_{k,k}vy_k(i-1) + Cl_{k,k}vy_k(i)$$

$$- Dl_{k,k}vy_k(i+1) + El_{k,k}vy_k(i+2)$$

$$= -\sum_{m=0,m \neq k}^{nk} \left\{ \begin{array}{l} Ar_{k,m}vy_m(i-2) - Br_{k,m}vy_m(i-1) + Cr_{k,m}vy_m(i) \\[2mm] - Dr_{k,m}vy_m(i+1) + Er_{k,m}vy_m(i+2) \end{array} \right\}$$

$$- \sum_{m=0}^{nk} \left\{ R_{k,m}\tau xx_m(ii-1) + S_{k,m}\tau xx_m(ii) \right\}$$

$$- \sum_{m=0}^{nk} \left\{ U_{k,m}\tau xy_m(i-1) + V_{k,m}\tau xy_m(i) \right.$$

$$\left. + W_{k,m}\tau xy_m(i+1) \right\} + Z_k. \qquad (30)$$

The following coefficients are presented for a regular grid with grid spacing *DY*. These coefficients do not change for different rheologies because they are formulated using the rheological coefficients. The coefficients $Ar_{k,m}$ to $Er_{k,m}$ are the same as coefficients $Al_{k,k}$ to $El_{k,k}$ except that everywhere the second index *k* is replaced by *m*:

$$Al_{k,k} = -\frac{1}{DY^4} RCxy3_{k,k}(i-1),$$

$$Bl_{k,k} = -\frac{2kwRCxx2_{k,k}(i-1)}{DY^2} - \frac{2RCxy3_{k,k}(i)}{DY^4} + \frac{RCxy1_{k,k}(i-1)}{DY^2}$$

$$- \frac{2RCxy3_{k,m}(i-1)}{DY^4} + \frac{k^2w^2RCxy3_{k,k}(i)}{DY^2},$$

$$Cl_{k,k} = -\frac{2kwRCxx2_{k,m}(i)}{DY^2} - \frac{2kwRCxx2_{k,m}(i-1)}{DY^2}$$

$$- \frac{RCxy3_{k,m}(i+1)}{DY^4} + \frac{2RCxy1_{k,m}(i)}{DY^2} - \frac{4RCxy3_{k,k}(i)}{DY^4}$$

$$- \frac{RCxy3_{k,k}(i-1)}{DY^4} + \frac{k^2w^2 2RCxy3_{k,k}(i)}{DY^2} - k^2w^2RCxy1_{k,k}(i),$$

$$Dl_{k,k} = -\frac{2kwRCxx2_{k,k}(i)}{DY^2} - \frac{RCxy1_{k,k}(i+1)}{DY^2} + \frac{2RCxy3_{k,k}(i+1)}{DY^4}$$

$$+ \frac{2RCxy3_{k,k}(i)}{DY^4} - \frac{k^2w^2RCxy3_{k,k}(i)}{DY^2},$$

$$El_{k,k} = -\frac{1}{DY^4} RCxy3_{k,k}(i+1), \qquad (31)$$

$$S_{k,m} = -\frac{2kw}{DY} RCxx4_{k,m}(i),$$

$$R_{k,m} = \frac{2kw}{DY} RCxx4_{k,m}(i-1),$$

$$U_{k,m} = \frac{RCxy4_{k,m}(i-1)}{DY^2},$$

$$V_{k,m} = \left(k^2 w^2 - \frac{2}{DY^2}\right) RCxy4_{k,m}(i),$$ (32)

$$W_{k,m} = \frac{RCxy4_{k,m}(i+1)}{DY^2},$$

$$Z_k = -4kw\dot{\varepsilon}_B \frac{\mu_k(i+1) - \mu_k(i-1)}{2DY}.$$

The solution of the system of algebraic equations provides the velocity harmonics vy_k, which are used to calculate the velocity v_y using eq. (14). The velocity v_x is calculated using eq. (15). For the calculation of the velocity field an implicit scheme is used because of the exponential growth of the amplification velocity with time, when the fold amplitudes are small. Furthermore, an adaptive time step strategy is used to control the motion of the layer boundaries, so as, for example, not to exceed a certain fraction of the smallest grid spacing. The marker points (400 points per layer boundary) that are fixed to the layer boundaries are moved by the calculated velocity field. Finally, the new layer boundaries define a new state of the system and the whole procedure is repeated to calculate again the corresponding velocities to further move the new layer boundaries.

VERIFICATION AND PERFORMANCE OF THE NUMERICAL CODE

The spectral/finite difference code is tested and verified for the initial stages of viscoelastic folding by the analytical solution derived in Schmalholz & Podladchikov (1999). The numerical solution agrees well with the analytical predictions in the initial stages (Fig. 4). Fig. 4 shows comparisons between the analytically and numerically calculated values of P, $\tau/(\tau^{nd} De)$ and A/A_0 versus the Maxwell time. Here, P is the layer-parallel stress, τ is the fibre stress, τ^{nd} is the fibre stress at $t=0$, $De = 2\mu_l e/G$ is the Deborah number, μ_l is the viscosity of the layer, e is the pure shear strain rate, G is the shear modulus of the layer, and A and A_0 are the current and initial fold amplitudes, respectively. The comparison is made for $R=1$, $\mu_l/\mu_m = 300$ and $De = 0.02$, where μ_m is the viscosity of the matrix. The parameter $R = [\mu_l/6\mu_m]^{1/3}(P/G)^{1/2}$ is designated as the dominant wavelength ratio and defines the folding mode for viscoelastic layers (Schmalholz & Podladchikov 1999). If $R>1$, folding of the compressed layer is dominantly controlled by the ratio of the layer-parallel stress to the shear modulus (P/G) and the viscoelastic layer behaves quasi-elastically. If $R<1$, folding of the compressed layer is dominantly controlled by the viscosity contrast (μ_l/μ_m) and the viscoelastic layer behaves quasi-viscously. Up to around three Maxwell time-scales the analytical and numerical results agree well. In Schmalholz & Podladchikov (2000) the numerical results are further compared with a new analytical solution for finite amplitude folding, and numerical and analytical results agree well up to threefold shortening.
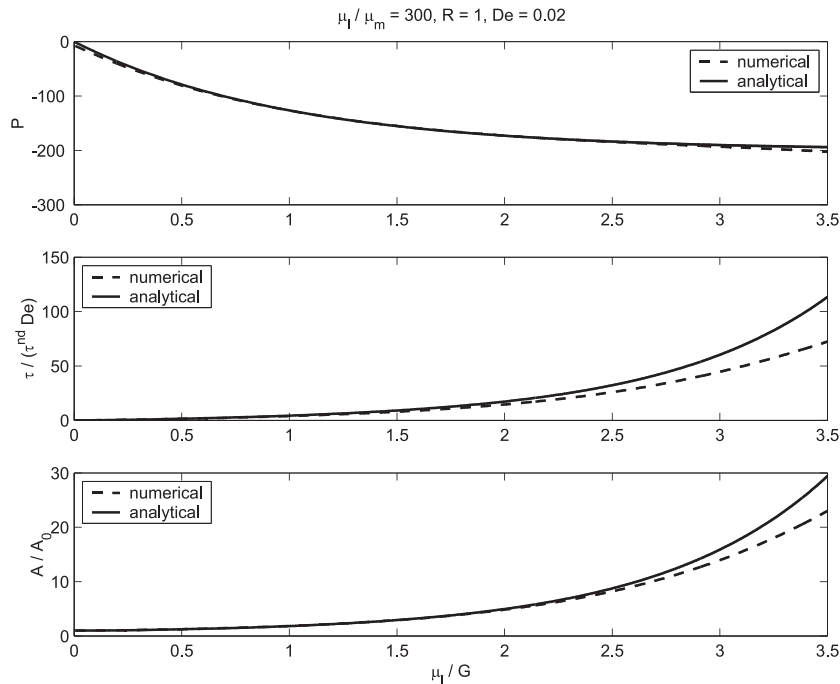
Figure 4. Comparison of analytical and numerical results for viscoelastic single-layer folding. The upper graph shows a plot of the increasing, compressive layer-parallel stress (P) versus the Maxwell time (ratio of viscosity to shear modulus μ_l/G). The middle graph shows a comparison of the normalized coefficients of the fibre stresses (τ), where τ^{nd} is the fibre stress at $t=0$ and De is the Deborah number (see text). After a few Maxwell time steps the analytical values grow faster than the numerical ones. The same tendency is observed in the lower graph, where the evolution of the ratio of initial to current fold amplitude (A/A_0) is shown.

The spectral method is frequently expected to be unsuitable for modelling systems with strong material heterogeneities due to the Gibbs phenomenon, which arises when the step function that describes the boundary between materials with different properties has to be approximated by trigonometric functions. However, the algorithm presented handled effective viscosity contrasts for folding simulations of up to 5×10^5 (Fig. 5b). Difficulties in modelling folding with very high viscosity contrasts also arise due to the very high growth rates of the fold amplitude, and not only due to the high viscosity contrast itself.

The spectral/FD method enables high performance of the numerical algorithm. A numerical calculation of heterogeneous viscoelastic flow (using a full upper convected formulation) with 1001 FD gridpoints, 64 spectral harmonics and 1000 time steps takes about 24 hr on a standard PC Pentium III (500 MHz). However, the numerical algorithm is currently not fully optimized and better performance is expected in the future.

EXAMPLES OF NUMERICAL SIMULATIONS

In the following the performance of the numerical algorithm is demonstrated by presenting the evolution of the pressure field during folding. The pressure is calculated using eq. (2) and is normalized by the product of the matrix's viscosity times the background strain rate (compressive pressures are negative). In all examples the layer boundaries were initially parallel to the shortening direction and exhibited a small initial geometric perturbation.

The pressure field is calculated for a folded, purely viscous single layer with viscosity contrasts of 500 (Fig. 5a) and 5×10^5 (Fig. 5b) and with a small initial sinusoidal shape of the layer boundary. The initial ratio of wavelength to layer thickness corresponded in both cases to 27, which corresponds to the dominant wavelength for a viscosity contrast of 500 (Biot 1961). The initial ratio of the fold amplitude to the layer thickness was 0.02. The pressure is presented for 77 per cent (Fig. 5a) and 74 per cent (Fig. 5b) strain [here strain is defined by $(\lambda_0 - \lambda)/\lambda_0$, where λ_0 and λ are the initial and current wavelengths of the folded layer, respectively]. The pressure field represents pressure perturbations on top of any background pressure field such as the lithostatic pressure. These two examples demonstrate that the spectral method is stable for large strains and for high viscosity contrasts.

In Fig. 6(a) a viscoelastic single layer ($R = 0.7$, $\mu_l/\mu_m = 100$) is presented that initially exhibited a random white-noise shape of the layer boundary. The distribution of the ratio $\max(\Delta\sigma)/P$ is shown, where $\max(\Delta\sigma) = (\tau_{xx}^2 + \tau_{xy}^2)^{1/2}$ and P is the pressure. The ratio $\max(\Delta\sigma)/P$ indicates how close the layer is to failure using a failure criterion $\max(\Delta\sigma) < \sin(\theta)P$. In this case, an angle of internal friction $\theta = 30°$ is assumed. Also, a specific normalized pressure value (here 203.8) is added to the calculated pressure perturbation to bring the layer in the initial stage close to failure [that is, to bring the initial values of $\max(\Delta\sigma)/P$ close to $\sin(30°) = 0.5$]. The white lines are contour lines for $\max(\Delta\sigma)/P = 0.5$. At 13 per cent bulk shortening, two failure areas (at the compressive parts of the fold hinges) are connected, indicating the development of a potential thrust within the fold limb, roughly between the inflexion points of the upper and lower layer boundary. The development of thrusts within fold

limbs was also observed for example by Gerbault *et al.* (1999). The failure areas are already disconnected again at 15 per cent strain (not shown), and for larger amplitudes (22 per cent) the failure areas start to increase at the parts of the fold hinges where extension takes place.

The pressure field is calculated for viscoelastic multilayers with $R = 2$ and $\mu_l/\mu_m = 2500$ (Fig. 7). The initial ratio of wavelength to layer thickness of the individual layers was 22 (this value corresponds to the dominant wavelength, Schmalholz & Podladchikov 1999) and the initial ratio of the amplitude to the layer thickness was 0.02. The thickness of the incompetent layers was equal to the thickness of the competent layers. At larger amplitudes an increase in maximum pressure in the fold hinges of the individual layers is observed from the top of convex-upward hinges of the whole sequence to the bottom of these hinges (Fig. 7a). This increase may result from a transmission of shear stresses through the multilayer sequence. In the multilayer sequence more shear deformation within the matrix occurs in the middle parts whereas at the margins of the sequence the matrix is less sheared (Fig. 7b). This causes the individual layers to show a more concentric fold shape at the margin of the sequence and a more chevron fold shape in the centre of the sequence. For large amplitudes (Fig. 7c), only the marginal layers show a concentric shape, whereas all other layers show a strong chevron shape. The fold limbs of the layers in the centre of the sequence are slightly folded.

The pressure field is calculated for viscoelastic multilayers with $R = 2$ and $\mu_l/\mu_m = 2500$ (Fig. 8), where the initial ratio of wavelength to layer thickness of the individual layers was 44 and the initial ratio of the amplitude to the layer thickness was 0.01. Also, the thickness of the incompetent layers was equal to the thickness of the competent layers. The fold shapes at 40 per cent (Fig. 8b) and 60 per cent (Fig. 8c) strain vary strongly between individual layers. Some layers within the sequence are dominated by extensive pressures whereas others are dominated by compressive pressures.

The numerical results shown in Figs 5, 7 and 8 were obtained using 1001 FD gridpoints and 64 spectral harmonics for the velocity, and the results shown in Fig. 6 were obtained using 1001 FD gridpoints and 128 spectral harmonics (movies of numerical simulations are available at http://www.geology.ethz.ch/sgt/staff/stefan).

SUMMARY AND CONCLUSIONS

The developed numerical code successfully simulates folding of viscoelastic multilayers up to large finite strains. The calculated fields of pressure and maximum differential stress are free of oscillations and demonstrate the applicability of spectral methods to physical systems with strong material heterogeneities. At small deformations, low-resolution Lagrangian finite element methods (FEMs) may be advantageous compared to our spectral-based method. This is due to the ability of the Lagrangian FEM mesh to follow material discontinuities, and the development of artificial oscillations about discontinuities that may result from spectral methods, i.e. the so-called Gibbs phenomenon. The Gibbs phenomenon is caused by the global character of the approximations, but was not observed in our calculations. However, mesh distortion resulting from large deformations results in low accuracy with Lagrangian FEM discretization methods (e.g. Braun & Sambridge 1995). This
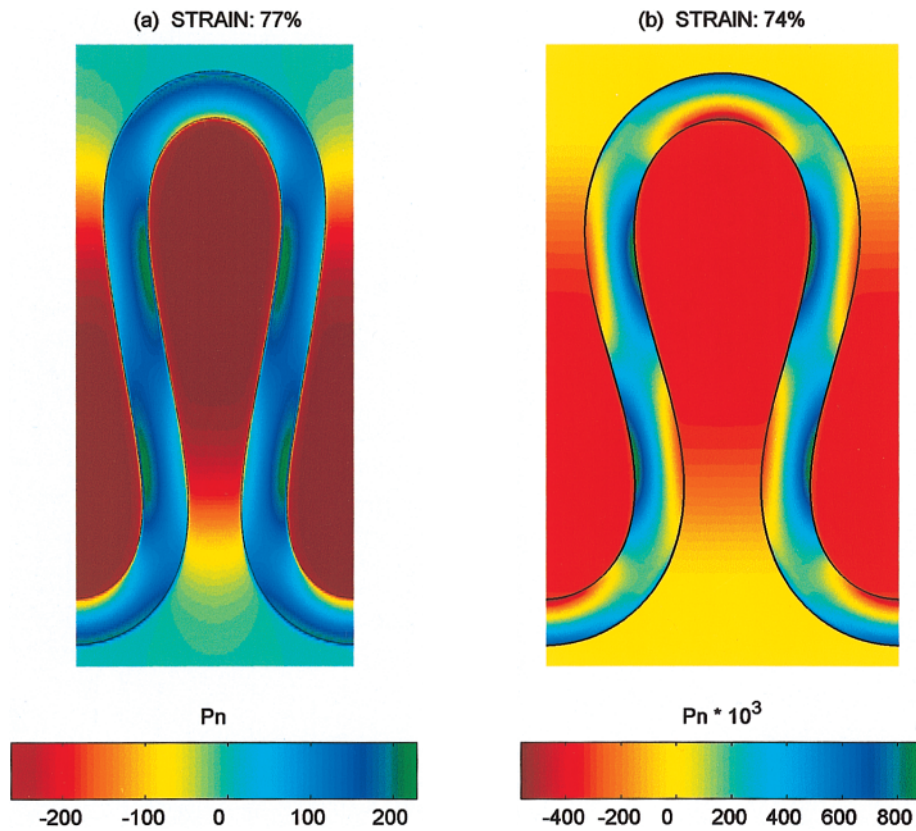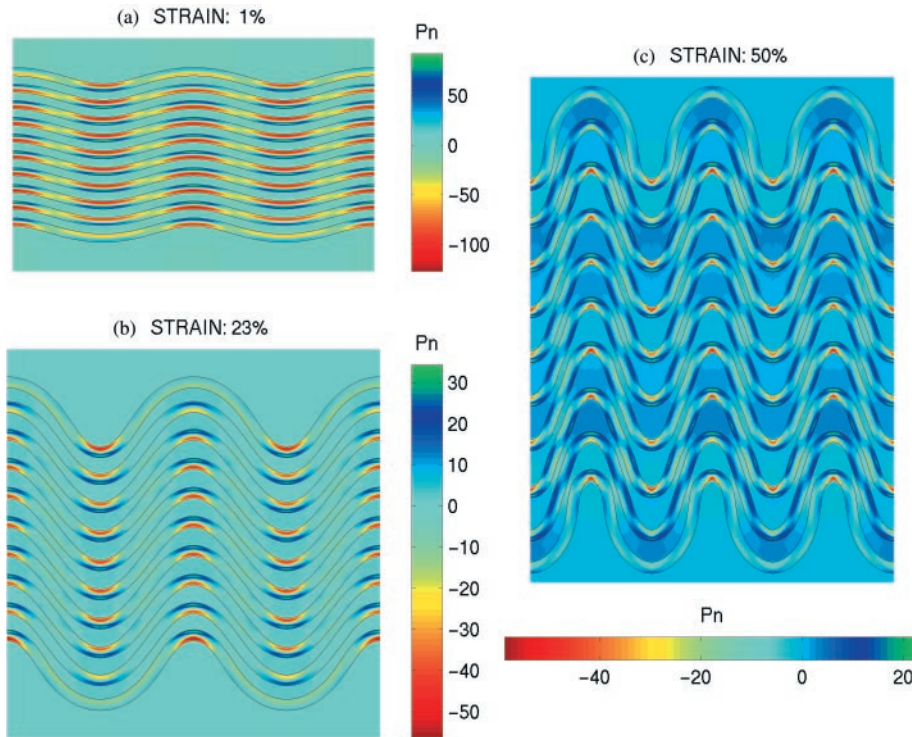
Figure 5. Pressure fields for large-strain viscous folding (compressive pressures are negative; $Pn = P/(\mu_m e)$ with P = pressure, μ_m = matrix viscosity and e = background strain rate). (**a**) Viscosity contrast is 500. (**b**) Viscosity contrast is 5×10^5. The calculated pressure fields are free of oscillations caused by the Gibbs phenomenon. In both simulations high compressive pressure builds up between the two fold limbs within the matrix (confined flow).
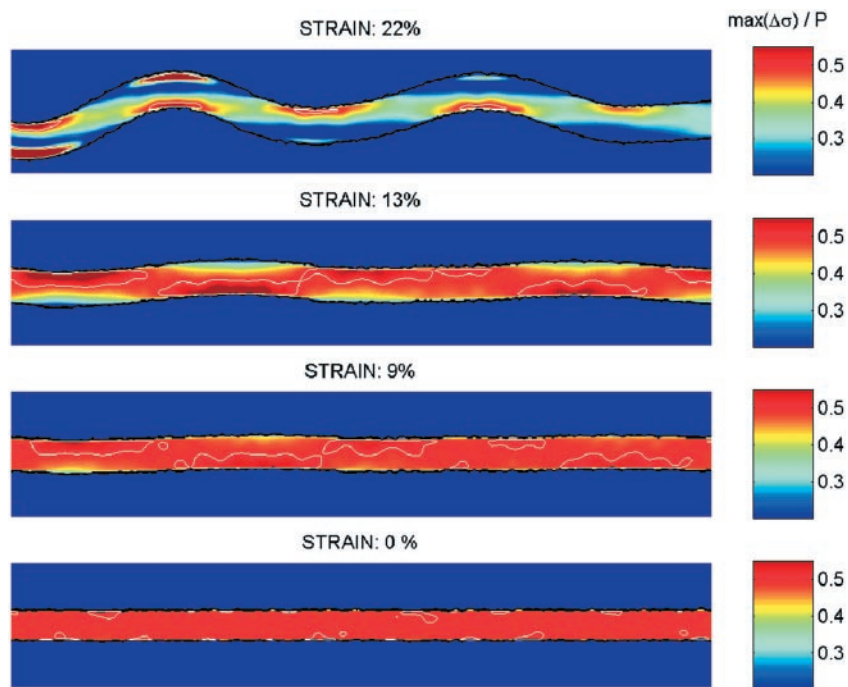

Figure 6. Distribution of the ratio of maximal differential stress to pressure [$\max(\Delta\sigma)/P$] for **a** viscoelastic layer ($R = 0.7$, $\mu_l/\mu_m = 100$) with initial random perturbation. White contour lines indicate $\max(\Delta\sigma)/P = 0.5$, which means failure would occur within the patches surrounded by the white lines. At 13 per cent strain two neighbouring failure areas are connected, indicating a thrust cutting through the whole layer within a limb. For larger strains, $\max(\Delta\sigma)/P$ increases at the parts of the hinges where extension takes place, indicating the development of extensive cracks.

Figure 7. Pressure distribution within viscoelastic ($R=2$, $\mu_l/\mu_m=2500$) multilayers (compressive pressures are negative; $Pn=P/(\mu_m e)$ with $P=$ pressure, $\mu_m=$ matrix viscosity and $e=$ background strain rate). Initial ratio of wavelength to thickness of individual layers is 22. (**a**) At 1 per cent strain strong pressure gradients appear in the fold hinges. (**b**) At 23 per cent strain the pressure field geometry within layers located in the middle of the sequence is different to that within layers located at the margin of the sequence. (**c**) At 50 per cent strain higher compressive pressures only appear within small areas within the fold hinge.
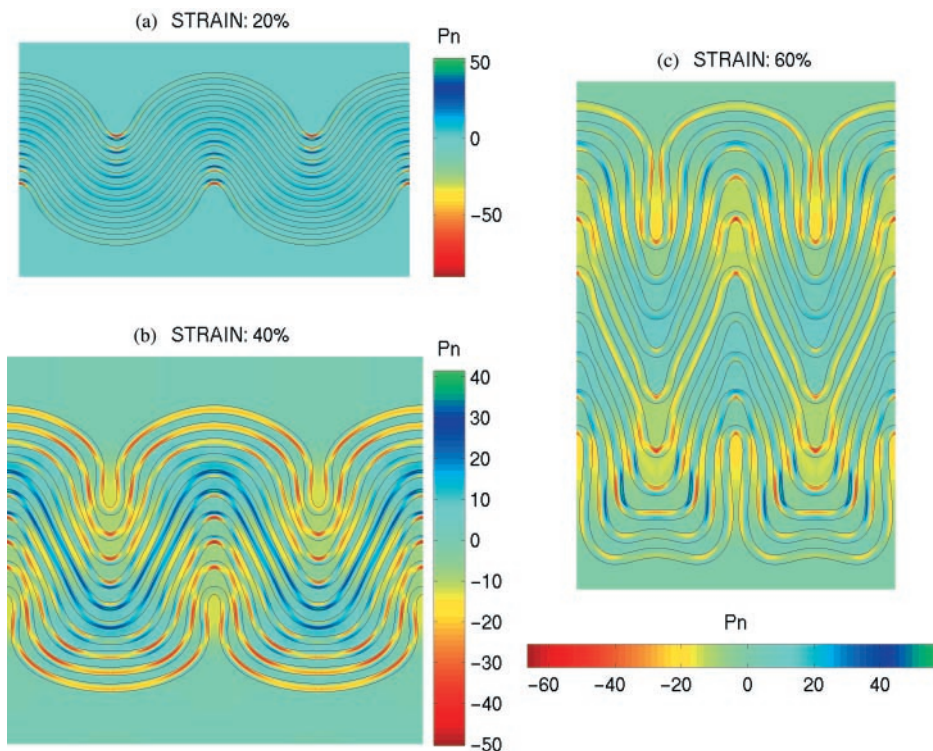
Figure 8. Pressure distribution within viscoelastic ($R=2$, $\mu_l/\mu_m=2500$) multilayers (compressive pressures are negative; $Pn=P/(\mu_m e)$ with $P=$ pressure, $\mu_m=$ matrix viscosity and $e=$ background strain rate). Initial ratio of wavelength to thickness of individual layers is 44. (**a**) At 20 per cent strain strong pressure gradients only appear within layers located at the margin of the multilayer sequence. (**b**) At 40 per cent strain the layers located in the middle of the sequence are dominated by extensive pressures. (**c**) At 60 per cent strain the individual layers show a complex geometry and significant pressure variations are also observed within the incompetent layers.

problem cannot be resolved by creating a new mesh because the interpolation of the stress tensor, which is sensitive to the orientation of the discrete element boundary, is an unsolved problem in large-strain numerical modelling by Lagrangian methods. The Eulerian formulation including complete objective derivatives of the stress tensor in the constitutive relationships used in this study avoids this problem.

According to our results for viscoelastic folding, the spectral/finite difference method combined with the Eulerian formulation is a promising numerical method to simulate dynamic processes that involve large deformations of heterogeneous, viscoelastic materials. Currently the algorithm is extended to include power-law rheologies also and to allow simulations of high simple shear deformations of heterogeneous materials, a deformation mode that is active during the formation of shear zones in rocks. The spectral/finite difference method is also suitable for 3-D simulations where two directions are treated with spectral methods and the third direction is treated with finite differences (e.g. Kaus & Podladchikov 2000). In future projects the spectral/finite difference method will be used to simulate mountain-building processes, in particular the evolution of the Alps.

ACKNOWLEDGMENTS

REFERENCES

Aris, R., 1962. *Vectors, Tensors and the Basic Equations of Fluid Mechanics,* Dover, New York.

Balachandar, S. & Yuen, D.A., 1994. Three-dimensional fully spectral numerical method for mantle convection with depth-dependent properties, *J. Comput. Phys.,* **113,** 62–74.

Biot, M.A., 1961. Theory of folding of stratified viscoelastic media and its implications in tectonics and orogenesis, *Geol. Soc. Am. Bull.,* **72,** 1595–1620.

Biot, M.A., 1965. *Mechanics of Incremental Deformations,* John Wiley, New York.

Borisenko, A.I. & Tarapov, I.E., 1968. *Vector and Tensor Analysis with Applications,* Dover, New York.

Braun, J. & Sambridge, M., 1995. A numerical method for solving partial differential equations on highly irregular evolving grids, *Nature,* **376,** 655–660.

Canuto, C., Hussaini, M.Y., Quarteroni, A. & Zang, T.A., 1988. *Spectral Methods in Fluid Dynamics,* Springer, Berlin.

Cobbold, P.R., 1977. Finite-element analysis of fold propagation: a problematic application?, *Tectonophysics,* **38,** 339–358.

Dieterich, J.H., 1970. Computer experiments on mechanics of finite amplitude folds, *Can. J. Earth Sci.,* **7,** 467–476.

Eisenhart, L.P., 1997. *Riemannian Geometry,* Princeton University Press, Princeton, NJ.

Fletcher, C.A.J., 1997a. *Computational Techniques for Fluid Dynamics,* Vol. 1, Springer, Berlin.

Fletcher, C.A.J., 1997b. *Computational Techniques for Fluid Dynamics,* Vol. 2, Springer, Berlin.

Fornberg, B., 1996. *A Practical Guide to Pseudospectral Methods,* Cambridge University press, Cambridge.

Fowler, C.M.R., 1990. *The Solid Earth,* Cambridge University Press, Cambridge.

Gerbault, M., Burov, E.B., Poliakov, A.N.B. & Daignieres, M., 1999. Do faults trigger folding of the lithosphere?, *Geophys. Res. Lett.,* **26,** 271–274.

Harder, H., 1991. Numerical simulation of thermal convection with Maxwellian viscoelasticity, *J. Non-Newtonian Fluid Mech.,* **39,** 67–88.

Huilgol, R.R. & Phan-Thien, N., 1997. *Fluid Mechanics of Viscoelasticity: General Principles, Constitutive Modeling, Analytical and Numerical Techniques,* Elsevier, Amsterdam.

Johnson, A.M. & Fletcher, R.C., 1994. *Folding of Viscous Layers,* Columbia University Press, New York.

Kaus, B.J.P. & Podladchikov, Y.Y., 2001. Forward and reverse modeling of the three-dimensional viscous Rayleigh-Taylor instability, *Geophys. Res. Lett.,* in press.

Kreyszig, E., 1991. *Differential Geometry,* Dover, New York.

Lan, L. & Hudleston, P.J., 1995. The effects of rheology on the strain distribution in single layer buckle folds, *J. struct. Geol.,* **17,** 727–738.

Mancktelow, N.S., 1999. Finite-element modelling of single-layer folding in elasto-viscous materials: the effect of initial perturbation geometry, *J. struct. Geol.,* **21,** 161–177.

Mase, G.E., 1970. *Continuum Mechanics,* McGraw-Hill, New York.

Oldroyd, J.G., 1950. On the formulation of rheological equations of state, *Proc. R. Soc. Lon.,* **A200,** 523–541.

Ramberg, H., 1981. *Gravity, Deformation and the Earth's Crust,* Academic Press, London.

Ramsay, J.G. & Huber, M.I., 1987. *The Techniques of Modern Structural Geology,* Vol. 2, *Folds and Fractures,* Academic Press, London.

Schmalholz, S.M. & Podladchikov, Y.Y., 1999. Buckling versus folding: importance of viscoelasticity, *Geophys. Res. Lett.,* **26,** 2641.

Schmalholz, S.M. & Podladchikov, Y.Y., 2000. Finite amplitude folding: transition from exponential to layer length controlled growth, *Earth planet. Sci. Lett.,* **181,** 619–633.

Sedov, L.I., 1960. Different definitions of the rate of change of a tensor, *Prik. Mat. I Mekh.,* **24,** 393–398.

Sedov, L.I., 1994. *Mechanics of Continuous Media,* World Scientific Publishing, Singapore.

Shashkov, M., 1996. *Conservative Finite-Difference Methods on General Grids,* CRC Press, Boca Raton, NY.

Simo, J.C. & Hughes, T.J.R., 1998. *Computational Inelasticity,* Springer, Berlin.

Tackley, P.J., Stevenson, D.J., Glatzmaier, G.A. & Schubert, G., 1993. Effects of an endothermic phase transition at 670 km depth in a spherical model of convection in the Earth's mantle, *Nature,* **361,** 699–704.

Turcotte, D.L. & Schubert, G., 1982. *Geodynamics. Applications of Continuum Physics to Geological Problems,* John Wiley, New York.

Zhang, Y., Hobbs, B.E. & Ord, A., 1996. Computer simulation of single-layer buckling, *J. struct. Geol,* **18,** 643–655.